Manifestation of Rayleigh Instability in Droplets Containing Multiply Charged Macroions

Styliani Consta*

Department of Chemistry, The University of Western Ontario, London, Ontario, Canada N6A 5B7

Received: December 23, 2009; Revised Manuscript Received: March 17, 2010

The Rayleigh limit and manifestations of instability in liquid droplets containing charged macroions are examined by molecular simulations. It is found that beyond the Rayleigh limit, the spherical droplets become unstable and form structures with distinct features. Regardless of the nature of the charged macroion, an assembly of spines of highly ordered polar solvent molecules form on the droplet surface. The surface charge distribution of the spiny droplet is highly nonuniform, and the macroscopic description of the droplet energy as a sum of electrostatic and surface terms is no longer valid. When the macroion is a charge-saturated polyhistidine chain, it is shown that the changes in the structure of the droplet are accompanied by the chain extension. Contrary to the conventional point of view, it is found that single ions present in droplets containing a highly charged macroion do not escape spontaneously but rather form complexes stable on the nanosecond time scale, depending on the degree of deviation from the Rayleigh limit and the nature of the ion. The effect of the instability in the disintegration mechanism of charged droplets in electrospray mass spectrometry experiments is discussed.

Introduction

Highly charged liquid droplets that contain solvent and an excess of ions of the same sign are ubiquitous in atmospheric aerosols found in thunder clouds or mists as well as in samples generated by electrospray (ES)[1] methods. In the last two decades, a great deal of knowledge about the physical and chemical processes that charged droplets undergo has been obtained in electrospray mass spectrometry (ESMS) experiments.[2−4] ES is employed to transfer analytes from solution into highly charged droplets that contain solvent, an excess of ions of the same sign, and analytes. These droplets carry thousands of excess unit charges contained in a volume with linear dimensions in the nanometer or micrometer range. Depending on the charge to volume ratio, the droplets release the extra charge by spontaneous fission[1,5] or an activated process.[6−8] A simple theoretical model that has often been used to determine the volume to charge ratio for spontaneous fission of a charged droplet is Rayleigh's model.[5] Rayleigh's model is a macroscopic model postulating that the total energy of the charged droplet is a sum of surface energy and electrostatic energy terms. The model further assumes that the droplet has constant volume and uniform electrostatic potential on the surface (the droplet is a conductor). Linear stability analysis with respect to small surface shape fluctuations leads to the following criterion that determines the spherical droplet stability

$$Q^2 = 64\pi^2\sigma\varepsilon_0 R^3 \qquad (1)$$

where Q, R, and σ denote the total charge of the droplet, the droplet radius, and the surface tension coefficient, respectively. Droplet fission at the critical droplet size defined by eq 1 is referred to as Coulomb explosion. The effect of simple ions on the stability of the charged droplets has been investigated in computer simulations[8−10] and was found to not affect significantly the criterion for droplet stability. We perform molecular simulations to address the validity of the Rayleigh model and consequently to examine the stability of liquid charged droplets when the charges are confined to a single macroion such as the peptide chain in the droplet. Active research in the field of ESMS in both experiments[11−15] and computations[16−19] focuses on the key question of explaining and finally predicting the charge state of a macromolecule in the gaseous state. In this article, the systems that we study are composed of solvent and macroions, and in the questions that we address, the solvent plays an integral role. To make connection with a realistic system accessible to experimental validation, we chose the model of a polyhistidine chain where every imidazole side chain carries a positive elementary charge embedded in a droplet of 1000 water molecules.

The effect of macroions on the morphology of charged droplets and their stability in accordance with the Rayleigh picture was addressed initially by Fenn[20,21] in his seminal studies of the detection of sodiated poly(ethylene glycol) (PEG) ions by ESMS. The PEG-$(Na^+)_n$ ions that were detected carried much higher charge than the Rayleigh prediction. Since the systems carry charge beyond the Rayleigh limit, the instability has to manifest itself in certain ways. Fenn[20,21] and de la Mora[14] proposed a model where the extension of the macroion is caused by Coulomb repulsion and, as a result, the droplet becomes elongated with conical ends that accumulate the charge density.

However, there is a spectrum of modifications that might lead to stabilization of the droplet. One plausible scenario is that beyond the Rayleigh limit, the solvent may solvate one charged end of the chain with charge close to the Rayleigh limit while the other end of the chain may protrude like a tail from the droplet by carrying away the rest of the charge. A schematic picture of this plausible scenario is shown in Figure 1a. This scenario is analogous to the way that a droplet that contains single charges fragments at the Rayleigh limit.[8] Another scenario is shown in Figure 1b, where the solvent solvates the charged chain in the form of beads in a necklace. For instance, a system of 1200 water molecules and 20 charges can form a necklace of beads where every bead contains 200 molecules that solvate

* E-mail: styliani.constas@gmail.com.

10.1021/jp912119v
Published on Web 04/06/2010

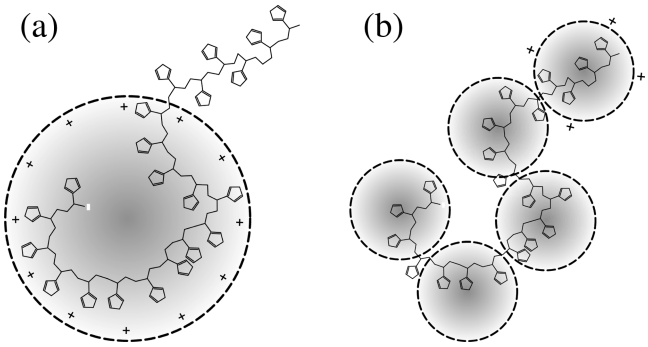

Figure 1. Possible morphology of a droplet that contains a macroion beyond the Rayleigh limit. A schematic representation of the solvent distribution around the polyhistidine chain is shown. The dashed circles represent the droplet surface. Induced charge at the droplet surface is indicated on some of the droplet surfaces. (a) Gradual expulsion of the charged segment from the droplet while the remainder of the chain in the droplet has the charge given by the Rayleigh model. The spherical droplet is stable according to the Rayleigh model. (b) Droplet shape consistent with the pearl mechanism of chain collapse.

5 charges in the chain, consistent with the Rayleigh limit. Even though these scenarios were not observed in the current simulations, they are consistent with the Rayleigh model and provide extensions for the instability of droplets in the presence of macroions. The validity of the scenarios will depend on the charge distribution on the chain, the effect of surface tension, solvent−solvent interactions, and solvation interactions between the solvent molecules and the ions.

System and Simulation Methods

Computer modeling was carried out using CHARMM[22] molecular simulation program. The water molecules were represented by the TIP3P[23,24] model with flexible bonds to capture salient features of surface tension.[25] No distance cutoffs were imposed on the forces. The temperature of the systems was maintained at 300 K using Berendsen's method[26] throughout the simulations. Throughout the simulations, a time step of 1 fs was used.

Charged Polyhistidine Chain in a Droplet. We studied the stability of droplets in the presence of macroions using direct MD simulations. To illustrate the phenomenon, we chose a model of a single polyhistidine peptide chain in a water droplet at low pH conditions. The clusters used in the simulations were comprised of 1000 water molecules and a single polyhistidine chain composed of 8−20 residues with charge from +8 (where e denotes the charge of a single proton) up to +20e, respectively. The droplet was contained in a spherical well of radius 10 nm. The low pH condition was modeled by protonating all of the side chains of the histidine residues. The carboxyl and amino groups at the ends of the chain were also charged as $-COO^-$ and $-NH_3^+$, respectively.

In the simulation, first, the longest relaxation time scale was determined. The water cluster containing the polyhistidine chain in a spherical droplet was relaxed in a 1 ns run. We verified that the simulation time is sufficient to complete relaxation of the radius of gyration and the accessible surface area. After a transient time, a labile stable state was attained. The configurations of the cluster were collected during a 5 ns production run. The collected trajectories were analyzed using CHARMM utilities. For every droplet configuration, a connected cluster containing the polyhistidine chain was determined. The connected cluster accessible surface area and the radius of gyration were computed as well as the corresponding probability distributions. The dynamic trajectories were farther analyzed to compute dipole−dipole radial distribution functions of the solvent.

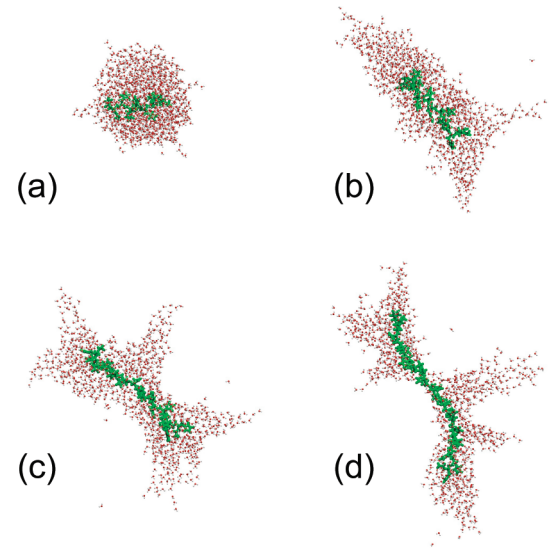

Figure 2. Typical snapshots of charged droplets that contain a polyhistidine of (a) 8 residues and $Z = 8e$, (b) 12 residues and $Z = 12e$, (c) 16 residues and $Z = 16e$, and (d) 20 residues and $Z = 20$ e in a droplet of 1000 water molecules. System (a) is below the Rayleigh limit, (b) slightly beyond the Rayleigh limit, and (c) and (d) in the Rayleigh instability regime.

Large Point Charge in a Droplet. We introduced a model of a heavy ion with mass 200 amu and Lennard-Jones parameters $\sigma_{LJ} = 0.4$ nm and $\varepsilon_{LJ} = 5.0$ kcal/mol. A series of 1 ns simulations have been carried out, with the charge of the ion ranging from +6e to +40e. We verified that all macroscopic parameters of the system were equilibrated on this time scale and computed surface and radius of gyration (RG) distributions of the connected clusters containing the single ion.

Single Ion in the Presence of a Polyhistidine Chain. Simulations of a droplet with 1000 TIP3P molecules containing a polyhistidine chain of 19 residues and a single ion of charge +1e were carried out. To examine the effect of the nature of the ion +1e in the simulations, we chose a model of a sodium cation as well as a protonated histidine. A multiple replica method[27] with 64 replicas was used to sample an ensemble of connected configurations of the system containing both the chain and the ion. The obtained ensemble of configurations was propagated in time to compute the average escape time for the ion. The results were compared with the fission time of a droplet containing 20 separate single ions.

Results and Discussion

Structure of Charged Droplets Containing a Macroion. Typical configurations of the systems that contain 8, 12, 16, and 20 residue chains in 1000 water molecules are shown in Figure 2a−d, respectively. The conformations of the chain depending on the charge that carries in combination with the behavior of the solvent are quantified by the RG of the chain and the surface area of the solvent. The histograms of the RG distribution are shown in Figure 3. The histograms of the RG show maxima at 7.5, 12, 15, and 21 Å for the chains of length 8, 12, 16, and 20 residues, respectively. The distributions for the 8 and 12 residue chains are broader relative to those of the 16 and 20 residue chains, which are sharp. The broader distributions reflect the larger freedom of the chains of 8 and

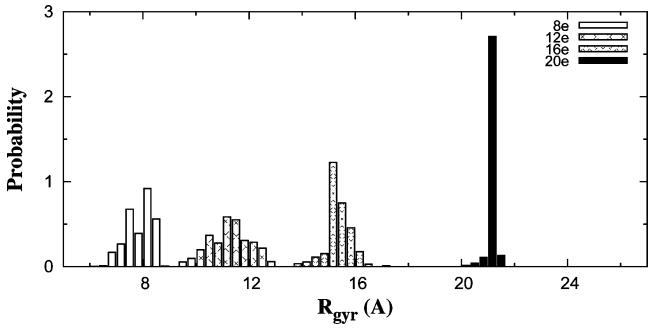

Figure 3. Probability distribution of the radius of gyration of a polyhistidine chain in a droplet of 1000 water molecules for the same systems as that in Figure 2.

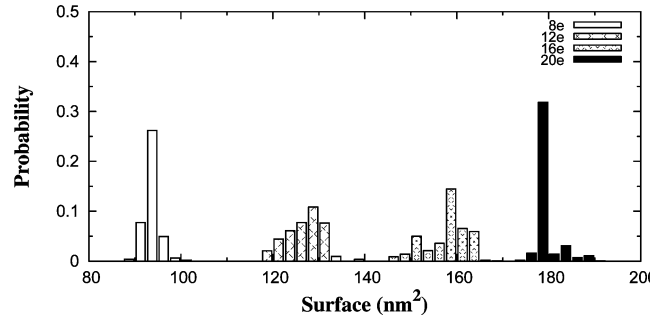

Figure 4. Surface area distribution for the same systems as those in Figure 2. The surface area of the droplet is determined according to Lee and Richards definition[29] as implemented in the CHARMM molecular modeling package.

12 residues to change their conformations relative to the fully extended rigid chains found in systems that contain 16 and 20 residues. The higher freedom in conformational changes for chains of 8 and 12 residues arises from the fact that the solvent carries away the charge of the chain; therefore, the repulsions within the charged groups of the chain are screened. In higher charged chains, the solvent is less effective in screening the repulsion of the residues, and as a result, the chains are extended.

Using computationally determined values for the RG, we compare the R_{gyr} distribution with that of ideal polymer models with correlated segment orientations $\langle \mathbf{R}_{C_\alpha C_\alpha}(i)\mathbf{R}_{C_\alpha C_\alpha}(i+1)\rangle > 0$. The corresponding Kuhn's lengths[28] (denoted by b_{Kuhn}) for the fitted models at different values of Z are given by

$$b_{\mathrm{Kuhn}} = \frac{6R_{\mathrm{gyr}}^2}{NR_{C_\alpha C_\alpha}} \tag{2}$$

where N and $R_{C_\alpha C_\alpha} = 0.378$ nm are the number of $C_\alpha - C_\alpha$ segments in the model ideal chain and the average C_α distance, respectively. The calculated Kuhn segment lengths are 2.9 ($Z = 8$e), 4.2 ($Z = 12$e), 7.0 ($Z = 16$e), and 13 nm ($Z = 20$e). The increase of the Kuhn segment lengths shows strong ordering of the $C_\alpha - C_\alpha$ orientations with the increase of charge.

For polyhistidine chain with $Z = +8$e, the Kuhn length is smaller than the chain length. As shown in Figure 2a, the chain is completely solvated and resides in the interior of the cluster. In approximately 70% of the conformations, the chain is compact. The droplets undergo shape fluctuations, forming incipient spine structures as well as short chains of ordered water molecules. The morphology of the clusters changes gradually as the charge of the chain increases by increasing its length. The 12 residue chain attains almost fully extended conformations in approximately 50% of the configurations and V-like conformations in the remaining configurations. A typical snapshot of the system is shown in Figure 2b, where the chain is extended and the solvent forms a conical shape in the one end of the droplet, while in the other end, it forms multiple cones. The chain lies completely in the interior of the droplet. In the majority of the configurations, the shape is asymmetric and is characterized by few large conical shapes in the ends of the chain or intermediate positions. In a significant portion of the configurations, the solvent molecules surround the chain in an ellipsoidal manner, forming a cone in one of the ends. For chains with charge +16e or larger, the Kuhn length is significantly higher than the chain length, and the polyhistidine chain backbone attains almost linear conformation. In the simulations, one observes development of multiple spines that are in a state of dynamic equilibrium. On the nanosecond time scale, the spines undergo a number of birth and collision events. In most of the configurations, the solvent forms pronounced spines along the chain (Figure 2c,d) that have finer structure of short water strings on their surface. The spines are predominantly but not exclusively concentrated on the ends of the chain, forming poorly solvated areas in the middle of the chain.

The picture that emerges is that as the charge of the droplet changes from +8e to +20e, the system passes progressively from an approximately spherical shape to an extended structure that is characterized by the formation of pronounced spines of ordered polar solvent molecules on its surface. The spines are in a dynamic equilibrium, and on the simulation time scale, we observe multiple spine collision, birth, and death events. The existence of spines can be rationalized as a way for the system to increase its effective radius beyond the Rayleigh limit and thus stabilize the system. As will be described in the next section, the formation of spines is typical of the multiply charged analyte and is independent of the distribution of the charge along the chain.

The effect of the spines on the surface area is shown in Figure 4. For 8, 12, 16, and 20 residue chains the average surface areas are 90, 125, 159, and 175 nm^2, respectively. The increase in the surface area cannot be attributed solely to the increase in the length of the chain. The dramatic increase in the surface area is mainly attributed to the increase of the number of spines as the charge increases. For the chains of 8 and 20 residues, the distribution of the surface area is sharp because the shape does not show dramatic deviations from the spherical shape and the elongated shapes, respectively, in the majority of the configurations. The chains of 12 and 16 residues show broader distributions because of the greater variability in the number of spines on the surface of the droplet.

In the simulations, we observed change in the solvent structure above the Rayleigh limit. Specifically, the solvent molecules became strongly oriented in the spines on the surface of the droplet. This change is significant as it changes the properties of the solvent and challenges the validity of the assumptions of the Rayleigh model. Using the "Radial Correlation Functions" module of the CHARMM molecular modeling package, we computed the dipole−dipole cumulative correlation function of the solvent. The dipole−dipole correlation function

$$D_Z(r) = \langle \sum_k ||\mathbf{d}_k||^2 \rangle^{-1} \sum_{(i,j):||\mathbf{r}_i - \mathbf{r}_j|| \le r} \mathbf{d}_i \cdot \mathbf{d}_j \tag{3}$$

gives the average normalized dipole moment of solvent molecules within the sphere of radius r. In eq 3, $\mathbf{d}_i$ and $\mathbf{r}_i$ denote

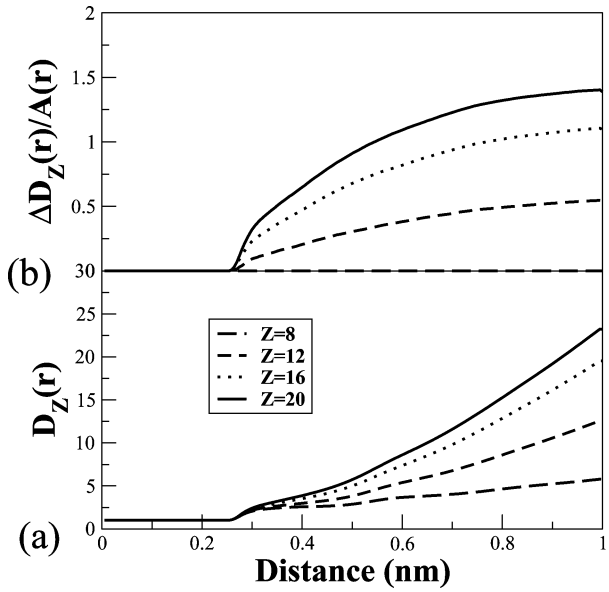

Figure 5. Dipole−dipole correlation function, $D_Z(r)$, dependence on droplet charge Z for the same systems as those shown in Figure 2.

the dipole moment and position of the center of mass of water molecule i, respectively. The summation in the numerator is carried over all pairs of water molecules closer than distance r. From the structure of the equation, one may easily establish that the quantity is equal to unity for small values of the radius (less than the first solvation shell) where only the dipole itself is present. If the solvent is polarized, the correlation function increases with the volume size, and in the absence of net polarization, the normalized function decays to zero. Figure 5a shows the dipole correlation function, D_Z, for the various charges, Z, and Figure 5b plots the difference $D_Z - D_8$ normalized by the surface area $A = 4\pi r^2$. Figure 5 shows that the ordering of solvent molecules becomes more pronounced as the charge of the system increases. The ordered domains are predominantly localized in the spines.

The electrostatic potential (ESP) at the vdW surface of the droplet due to the macroion and solvent is shown in Figure 6a−d. In the same figure, the field lines due to solvent only are also presented. The electrostatic potential for systems with the macroion of $Z = +8e$ shows variations in the range of 3 kcal/mol. Figure 6a for systems below the Rayleigh limit shows that the Rayleigh assumption of uniform electrostatic potential over the surface is valid even though the charge is connected and is found in the interior of the system. The field lines are closed loops that predominantly connect amino and carboxyl termini of the polyhistidine chain. As the charge of the ions increases, the deviations in the ESP on the surface increase as well to approximately 30 kcal/mol for $Z = +20e$. Nevertheless, the value is still considerably smaller than the value of the electrostatic potential $E = 666.4$ kcal/mol of a point charge $Z = +20e$ at 1 nm. The ESP reaches its minimum on the tips of the spines and is maximum in the saddle points between the spines as well as in intermediate parts of the body of the droplet that are the closest to the macroion groups. The ESP shows significant deviations from the isopotential approximation of the Rayleigh model. The induced solvent electrostatic potential demonstrates the presence of an ordered state of water in the droplet. The field lines of the solvent-induced electrostatic field show charge transfer by the polar solvent to the tips of the spines.

The simulations reported above were carried out with the polyhistidine chain as a realistic example of a multiply charged

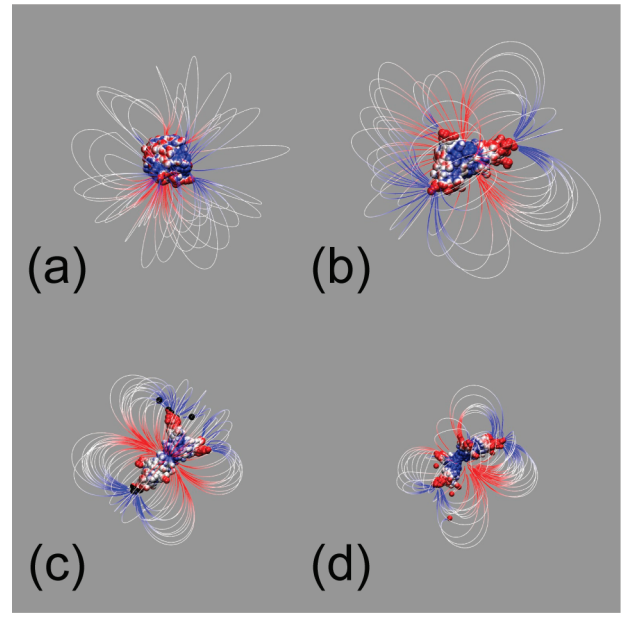

Figure 6. Electrostatic potential of the entire system and field lines of the solvent-induced electrostatic field for the same systems as those in Figure 2. The red regions on the vdW surface of the droplet represent low potential and the blue high.

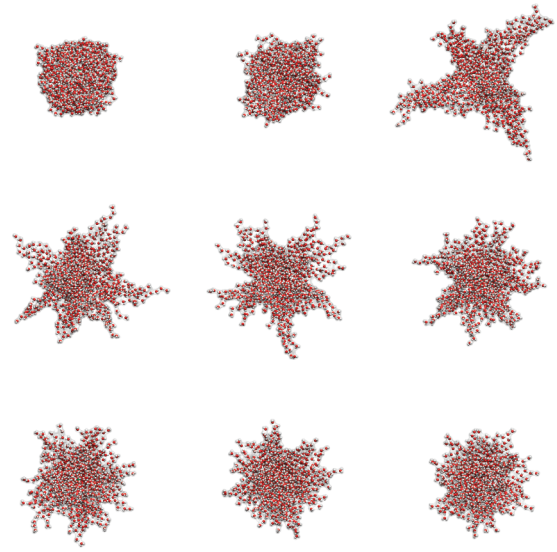

Figure 7. Droplet conformations in a presence of a single fictitious charged ion. The total charges of the droplets are $Z = \{6, 10, 14, ..., 38\}$.

ion. However, the solvent structure around an ion with charge beyond the Rayleigh limit is universal and does not depend on the nature of the ion. The results of simulations of TIP3P solvent around a charged center with charges varying from $Z = +6e$ to $+38e$ are presented in Figure 7. The solvent conformations look remarkably similar to the conformations of the solvent around the polyhistidine chain. The RG and the surface area shown in Figure 8 reveal the discontinuity above the Rayleigh limit. As the charge of the system increases, the structures become more compact with the increasing number of spines. We would like to emphasize that the solvent surface can not be rationalized on the basis of macroscopic description in terms of extrema of the energy functional of surface and electrostatic terms. In the tips of the spines, the surface tension pressure is infinite, and hence, new functional forms of surface energy are called for.

Single Macroion and an Ion in a Droplet. We assessed the stability of a system containing both the polyhistidine chain and

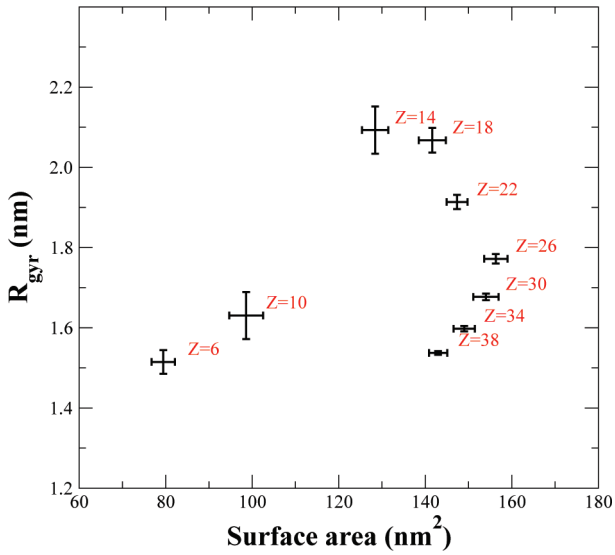

Figure 8. Average surface area and radius of gyration of charged droplets from Figure 7.

a single ion above the Rayleigh limit. To study the effect of the droplet configuration on the rate of escape of the single ion from the droplet, an array of simulations was carried out on a test system of a cluster of 1000 water molecules that contain an 11 residue polyhistidine chain and a sodium ion, adding to the total charge of +12e.

A droplet containing 1000 water molecules and 12 ions is highly unstable. If the ions are not covalently bonded, the droplets undergo the first fission event in less than 20 ps depending on the initial configuration. The cascade of fission events rapidly reduces the charge of the main droplet to +6−7e. The rate of droplet disintegration does not depend on the nature of the constituent ions and was approximately the same for sodium and histidine ions. In contrast to the fission of the droplet with discrete charges, the system that contains an 11 residue polyhistidine chain and a single ion is stable on the 100 ps time scale, and the rate of ion escape depends on the nature of the ion. In the course of simulations, we equilibrated systems containing the polyhistidine chain and the ion using the hybrid Monte Carlo (HMC) method.[30] In the acceptance rule, we disallowed fragmented configurations. The generated ensemble of connected configurations was evolved for $\tau = 2$ ps. The rate of escape R_f of the sodium ion from the droplet was estimated from the portion of the fragmented configurations in the ensemble C_{frag} as

$$R_f = C_{frag}/\tau = 1.6\text{ns}^{-1} \quad (4)$$

The escape of an ion is a complex process involving spine formation with the ion at the spine base and subsequent slow diffusion of the ion to the tip of the spine. When the single ion is histidine, the rate of escape is much slower. This decrease is presumably due to a much larger radius of the histidine molecule as compared with that of the sodium ion. The slower diffusion of the histidine molecule to the spine tip makes the escape rate an order of magnitude smaller.

Conclusions

The instability beyond the Rayleigh limit was investigated in droplets that contain a highly charged macroion. It was found that the solvent that surrounds the ion forms structures resembling in shape a sea urchin. The spines reduce the electrostatic interactions in the droplet by transferring the charge on the tips of the spines and, hence, spreading it over a larger surface. The assembly of spines has a striking resemblance to isopotential surfaces that have singularities in charge density. The variations of the electrostatic potential on the surface of the droplet and the formation of the tips precludes the use of the assumptions of the Rayleigh model to express the energy of the system.

The spiny structures give rise to unique behavior of the unstable system. Intuitively, one would expect that any additional single charge in a droplet that contains a macroion with charge beyond the Rayleigh limit will escape readily. However, simulations show that the system stays connected for up to nanoseconds before it releases the single ion. The reason for the slowdown of the escape rate of the ion is that the formation of a highly ordered state of the polar molecules in the spines prevents the solvation of the single ion. Unlike the case of Coulomb explosion, the rate of single ion escape strongly depends on the nature of the ion. The difference was demonstrated by studying the escape of a sodium ion versus a protonated histidine. In addition, it has been observed that solvent evaporation from the droplet is arrested. Only a few solvent evaporation events take place over a 1 ns run.

In addition to the study of the fundamental problem of the validity of the Rayleigh model in droplets that contain charged macroions, our studies provide insight into the charge state of coiled macroions in droplets generated by ES. When the droplet is much larger than the macroion, it disintegrates by solvent evaporation and conventional Coulomb explosions. From the Rayleigh expression (eq 1), one deduces that the pH of the droplet reduces by 1.5 when the radius of the droplet is reduced by an order of magnitude. Since a droplet of radius ∼10 nm is composed of $\sim 10^{15}$ water molecules, it is safe to assume that thermodynamic theories hold; therefore, the charge on the macroion is determined by the chemical equilibrium with the protons. For a droplet of this size, the pH is 1.3, which is sufficiently low to protonate all of the basic sites of a coiled peptide. The rate of proton transfer will play a dominant role in the charge state of the macroion if it is slower than the droplet disintegration rate. When the droplet size will be a few layers thick around the macroion, there will only be a handful of single ions available in the solvent. For instance, in a droplet of 2 nm, a polyhistidine of 10 residues will carry charge +10e, and there will be a single proton in the droplet. The polyhistidine chain will have coiled conformation in the droplet, even though it carries high charge. Once the droplet becomes smaller because of solvent evaporation, the charge of the polyhistidine chain may exceed the Rayleigh limit. This argument is supported by the observation of metastable states above the Rayleigh limit formed by the macroion and single ions and computations of the free-energy profiles for the fragmentation of $Ca^{2+}-2Na^{+}$ in 170 water molecules.[8] At later stages, the chain extends, and spine-like structures develop on the surface of the solvent. Notwithstanding the slowing of the solvent evaporation rate, deprotonation events might still occur since this will allow the system to release the charge. However, the escape of the single proton will be delayed due to the spiny structures of the solvent around the microion. As a result, the macroion will emerge by carrying higher charge for its size relative to the Rayleigh prediction. Our results are in qualitative agreement with the suggestions of Fenn[20,21] and de la Mora;[14] however, simulations show a more complex picture of the structure of the droplets beyond the Rayleigh limit, with implications in the dynamics of the escape of ions. The role of the conformations of the

molecule, the basicity of the solvent, and experimental parameters such as collision rates between the macroion and solvent molecules on the charge state of a macroion have been examined.[19,31,32] In addition to the above factors, we demonstrated that increased stability beyond the Rayleigh limit of droplets containing a multiply charged macroion may also be a factor that affects the charge state of a macroion. Furthermore, the ordered structure of solvent that surrounds the macroion might affect the proton-transfer mechanism in a way different from what has been assumed in the used thermodynamic models. Currently, we address the effect of charged environment on the mechanism and dynamics of proton exchange between a polyhistidine chain and the solvent.

Acknowledgment. S.C. thanks the Discovery Grant and the Accelerator Grant for Exceptional New Opportunities (AGENO) of Natural Sciences and Engineering Research Council of Canada (NSERC) for funding this research and SHARC-Net for providing the computing facilities to perform the simulations.

References and Notes

(1) Dole, M.; Mack, L.; Hines, R.; Mobley, R.; Ferguson, L.; Alice, M. *J. Chem. Phys.* **1968**, *49*, 2240–2249.

(2) Kebarle, P.; Verkerk, U. H. *Mass Spectrom. Rev.* **2009**, *28*, 898–917.

(3) Hogan, Jr., C. J.; de la Mora, J. F. *Phys. Chem. Chem. Phys.* **2009**, *11*, 8079–8090.

(4) Nguyen, S.; Fenn, J. B. *Proc. Natl. Acad. Sci. U.S.A.* **2007**, *104*, 1111–1117.

(5) Rayleigh, L. *Philos. Mag.* **1882**, *5*, 184–186.

(6) Iribarne, J.; Thomson, B. *J. Chem. Phys.* **1976**, *64*, 2287–2294.

(7) Thomson, B.; Iribarne, J. *J. Chem. Phys.* **1979**, *71*, 4451–4463.

(8) Consta, S.; Mainer, K.; Novak, W. *J. Chem. Phys.* **2003**, *119*, 10125–10132.

(9) Consta, S. *J. Mol. Struct.* **2002**, *591*, 131–140.

(10) Ichiki, K.; Consta, S. *J. Phys. Chem. B* **2006**, *110*, 19168–19175.

(11) Peschke, M.; Verkerk, U.; Kebarle, P. *Eur. J. Mass Spectrom.* **2004**, *10*, 993–1002.

(12) Verkerk, U.; Peschke, M.; Kebarle, P. *J. Mass Spectrom.* **2003**, *38*, 618–631.

(13) Blades, A.; Peschke, M.; Verkerk, U.; Kebarle, P. *J. Phys. Chem. A* **2002**, *106*, 10037–10042.

(14) de la Mora, J. F. *Anal. Chim. Acta* **2000**, *406*, 93–104.

(15) Williams, E. *J. Mass Spectrom.* **1996**, *31*, 831–842.

(16) Segev, E.; Wyttenbach, T.; Bowers, M. T.; Gerber, R. B. *Phys. Chem. Chem. Phys.* **2008**, *10*, 3077–3082.

(17) Jortner, J.; Last, I.; Levy, Y. *Int. J. Mass Spectrom.* **2006**, *249*, 184–190.

(18) Schnier, P.; Price, W.; Williams, E. *J. Am. Soc. Mass Spectrom.* **1996**, *7*, 972–976.

(19) Schnier, P.; Gross, D.; Williams, E. *J. Am. Soc. Mass Spectrom.* **1995**, *6*, 1086–1097.

(20) Nohmi, T.; Fenn, J. *J. Am. Chem. Soc.* **1992**, *114*, 3241–3246.

(21) Fenn, J.; Rosell, J.; Nohmi, T.; Shen, S.; Banks, F. Electrospray Ion Formation: Desorption versus Desertion. In *Biochemical and Biotechnological Applications of Electrospray Ionization Mass Spectrometry*; Snyder, A. P., Ed.; American Chemical Society: Washington, DC, 1996; Vol. 619.

(22) Brooks, B.; Bruccoleri, R.; Olafson, B.; States, D.; Swaminathan, S.; Karplus, M. *J. Comput. Chem.* **1983**, *4*, 187–217.

(23) Neria, E.; Fischer, S.; Karplus, M. *J. Chem. Phys.* **1996**, *105*, 1902–1921.

(24) Jorgensen, W.; Chandrasekhar, J.; Madura, J.; Impay, R.; Klein, M. *J. Chem. Phys.* **1983**, *79*, 926–935.

(25) Alejandre, J.; Tildesley, D.; Chapela, G. *J. Chem. Phys.* **1995**, *102*, 4574–4583.

(26) Berendsen, H.; Grigera, J.; Straatsma, T. *J. Phys. Chem.* **1987**, *91*, 6269–6271.

(27) Malevanets, A.; L. Sirota, F.; Wodak, S. *J. Mol. Biol.* **2008**, *382*, 223–235.

(28) Doi, M.; Edwards, S. *The Theory of Polymer Dynamics*; Oxford University Press, New York: 1988.

(29) Lee, B.; Richards, F. *J. Mol. Biol.* **1971**, *55*, 379–380.

(30) Duane, S.; Kennedy, A.; Pendleton, B.; Roweth, D. *Phys. Lett. B* **1987**, *195*, 216–222.

(31) Iavarone, A.; Jurchen, J.; Williams, E. *Anal. Chem.* **2001**, *73*, 1455–1460.

(32) Iavarone, A.; Jurchen, J.; Williams, E. *J. Am. Soc. Mass Spectrom.* **2000**, *11*, 976–985.

JP912119V